The wheat straw biochar research on the adsorption/desorption behaviour of mercury in wastewater

Shici Zhang [1], Zejiao Luo [2*], Mohammed A. S. Abdalla [2,3], Shibin Xia [1*]

[1] School of Resources and Environmental Engineering, Wuhan University of Technology, Wuhan, 430070, China
[2] School of Environmental Studies, China University of Geosciences (Wuhan), Wuhan, 430074, China
[3] Department of Soil and Water Science, College of Agriculture, University of Bahri, Khartoum, 1660, Sudan

*Corresponding author:
zjluo@cug.edu.cn; Tel.: +86-134-7621-2088
xiashibin@126.com; Tel.: +86-153-9288-0268
Presenting author email: zhangshici@whut.edu.cn; Tel.: +86-186-7238-0657

Abstract: Biochar is a cost-effective and eco-friendly adsorption material that has been wildly used in heavy metal removal studies. However, broad and comprehensive studies are yet to expound on the behavior and mechanism of Hg(II) adsorption and desorption onto biochars derived from different pyrolysis temperatures. This study exploits a approach on the utilization of biochar derived from season wheat straw in the treatment of simulated mercury-containing wastewater. The physical characteristics of biochar were analyzed using BET and SEM. It was found that high temperature biochar had an obvious micropore development and a BET specific surface area of 55.92 m^2/g. The adsorption isotherm characteristics of three kinds of biochars were extensively described through Langmuir isothem (R^2 > 0.9782) and pseudo second-order kinetics (R^2 > 0.9421), with the maximum theoretical adsorbing capacity measured at 5.85, 4.13 and 3.56 mg/g respectively in the following order: WBC300 > WBC400 > WBC600. In binary wastewater systems, when Pb(II) initial concentration was 10 mg/L, Pb(II) and Hg(II) competed for adsorption sites, leading the removal efficiency for Hg(II) was 18.0% lower than that of a single mercurial system. Complexation reactions with acidic surface functional groups were estimated in the Hg(II) adsorption process onto WBC300 and WBC400. It was then confirmed by the results of FT-IR and water-soluble cation test that low temperature biochars (WBC300 and WBC400) adsorbed Hg(II) mainly relied on complexation reactions with oxygen-containing functional groups such as carboxyl, alcoholic and phenolic hydroxyl, while high temperature biochars (WBC600) mainly relied on ion-exchange interactions. This research proposes a novel and potential method for mercury-containing wastewater treatment and simultaneous remediation of mixed heavy metals.

Keywords: wheat straw, biochar, mercury-containing wastewater, adsorption, desorptio

1. Introduction

Mercury (Hg), being one of the high toxicity heavy metals, is mainly present in the global environmental chemical cycle in its gaseous phase, which potentially causes problems including contamination that may lead to pollution, poisoning, and other human diseases [1]. Mercury can also be released into the aquatic environments via natural and anthropogenic processes. Volcanic eruptions, tectonic activities, and rock weathering are three main natural approaching, for artificial emission pathways, on the other hand, including coal combustion, chlor-alkali processing, mining, oil refining, electroplating, and battery, paint, and paper manufacturing [2, 3]. It is reported that China as the largest coal-consuming country, discharged mercury at an annual estimated rate at 25% to 40% of the global total emissions [4]. Mercury is present in the environment in three forms which include elemental mercury (Hg^0), inorganic mercury (Hg^+, Hg^{2+}), and organic mercury, all of which are toxic to humans. Hg^0, Hg^+ and Hg^{2+} have relatively low toxicity to cause nausea, abdominal pain, as well as nephritic and hepatic degeneration. Hereinto, Hg^{2+}, in its predominant valence of methylation, forms methylmercury which is a lead cause of nervous system damage due to the bioaccumulation through food chain, passage of the blood-brain barrier, and damage of the placental barrier, which may cause excessive salivation, memory loss, tremor, and birth defects in infants [5-7]. In the awareness of its health hazards and contaminant issues, the United Nations Environment Programme (UNEP) led the Minamata Convention concerning mercury in 2013, which was attended by 128 countries [8]. China as one of the signatories, agreed to regulate the emission standards for industrial mercury-containing wastewater under the constraints of the convention, in such case, the Emission Standard of Pollutants for Battery Industry (GB 30484-2013) was issued by the government that led to a stipulated of the mercury emission limits of existing facilities to be raised from 0.02 mg/L to 0.005 mg/L, while for environmentally vulnerable areas, mercury emissions should be less than 0.001 mg/L, effective on January 1st of 2016. This is the main reason why researches on the remediation and treatment of mercury-containing wastewater has become a priority in the heavy metals prevention and control not only in China but in the entire world.

Several techniques of wastewater treatments for the removal and regulation of mercury emissions in aquatic environments are already available. Among these techniques include chemical precipitation (co-precipitation, sulfide precipitation, etc.) [9, 10], electrolytic method via electrocoagulation [11, 12], ion exchange procedures [13, 14], and other biological methods [15, 16].These measures, however, display several downsides such as the need for a relatively long reaction time, production of solid residues, and the cause of secondary contamination [17]. Moreover, physical and chemical adsorption techniques are currently garnering attention in the research field as it makes use of a simple device and operation process that has already been wildly studied and it also uses a number of adsorbents which are proven to be efficient in mercury adsorption including oxidizing materials (metal oxides, magnetic graphene oxides, etc.) [18-20], minerals (zeolites, vermiculites, etc.) [4, 21], chelating fiber [22], carbon nanotubes [23, 24], and the most common adsorbent being activated carbon and its derivatives [25, 26]. The industrial large-scale application of these adsorbents are all limited due to their complex production process, method of activation, high energy consumption, even the crude material cost. However, the evolution of biochar from an activated carbon alternative to a pyrolytic black carbon adsorbent, derived from naturally renewable biomass, received increasing attention in recent years due to its bargain price, high efficiency and environmentally friendly traits in mercury-containing wastewater remediation [3, 27].

Different from activated carbon, biochar is produced via thermal pyrolysis with limited oxygen or inert gas conditions under relatively low temperature (less than 700°C). The characteristics of biochar as porous, carbon-rich, fine-grained, and bearing a variety of chemical composition and surface functional

groups are related to its production environment and raw material generation, which can be divided into crop straw, wood, poultry manure, animal bones, and so on that mainly roots in agriculture, forestry, and animal waste, thereby further affecting the adsorption performance of the substance [28-33]. Multiple studies regarding biochar adsorption on heavy metal wastewater treatment have been previously reported, but majority of the articles focused on single metal like Pb^{2+}, Cd^{2+}, Cu^{2+}, Zn^{2+}, Cr^{3+} and Cr^{6+}. On the other hand, the concern about the adsorption and desorption behaviour of biochar on Hg(II) has been very rare and only a few research has been found tackling the topic [34, 35]. Few authors have expounded on the metal effects like Hanandeh et al. [34] who prepared biochar from Jordanian olive oil processing solid waste and found that the adsorption capacity of Hg(II) have increased with the improvement of its pyrolysis temperature, therefore the resulting maximum capacity was 104.59 mg/g with a terminal temperature of 630°C according to his findings. Nevertheless, the Brazilian pepper biochar reflected an opposite tendency by which the higher the pyrolysis temperature generated, the lower the resulting Hg(II) adsorption capacity. In this matter, the maximum capacity occurred at 24.2 mg/g with a biochar pyrolysis temperature of 300°C [2]. This indicates that the biochar adsorption capacity of Hg(II) shows a relationship with the sources of biomass and the initial mercury concentration. Moreover, Xu et al. [36] compared Hg(II) adsorption characteristics and mechanisms of two biochars samples which were obtained from dried bagasse and hickory chips pyrolyzed at 450°C for 2 h and another commercial activated carbon. Their results showed that biochars had better adsorption capabilities than activated carbon by the substances' complexation and Hg-π binding with functional groups. In the case of co-sorption of phenanthrene and mercury, Kong et al. [37] and Tang et al. [38] investigated soybean stalk-based and graphene biochar respectively, their findings concluded that biochar still evidently revealed prospects in the co-sorption application despite the polycyclic aromatic hydrocarbon and mercury bearing a competitive sorption mechanism in the binary solution. To sum up, the adsorption/desorption behaviour of Hg(II) and the co-sorption with other heavy metal ions in the binary systems has not been fully elaborated and comprehensively studied yet.

As discussed in the statement above, the overall objective of this research is to explore and elaborate the mechanisms of Hg(II) adsorption by biochars through a series of adsorption/desorption experiments. In china, the total yield of straw ranks first all around the world with an annual output of more than 800 million tons, in which global wheat straw production occupies in an estimated rate of more than 12% [39]. In our study, the acquisition of a series of wheat straw biochars are to be used for the integration of agricultural waste management towards heavy metal wastewater treatment. These wheat straw biochars were obtained via slow pyrolysis in nitrogen atmosphere at 300 to 600°C. The batch experiments were able to identify the behaviour of biochars in mercury adsorption/desorption, these were done in combination with empirical models and characterization techniques such as Brunauer-Emmett-Teller (BET), Scanning Electron Microscopy (SEM), X-ray Fluorescence (XRF), X-ray Diffraction (XRD) and Fourier Transform Infrared Spectrometer (FT-IR), and further acquired insights of Hg(II) removal mechanism.

2. Materials and methods

2.1. Preparation of wheat straw biochars

Fresh wheat straw were collected from Hannan district, Wuhan, China (114.04°E, 30.29°N), these were initially washed three times to remove surface dust or insect debris, then oven-dried (DHG-9240A, Sanfa Scientific Instruments Co., Ltd, China) at 105°C for 12 h. This was then continuously fed with N_2 at a flow rate of 60 mL/min for half an hour to achieve an oxygen-free environment. The specified

pyrolysis temperature of the vacuum tube furnace (TF-1200X, Hefei Ke Jing Materials Technology Co., Ltd, China) reached 300°C, 400°C, and 600°C respectively at the heating rate of 10 °C/min which was then maintained on the entire procedure for up to 2 h. After that, N_2 was constantly fed through the vacuum tube until the biochar was cooled to room temperature. Finally, the product was passed through a 60 mesh sieve (with a size less than 0.25 mm) and then referred as BC300, BC400 and BC600.

2.2. Characterization of wheat straw biochars

For the purpose of studying the physico-chemical properties of the BC samples, the yield, net yield (as equation 2-1 and 2-2 presents), ash content, and pH (followed National Standards of People's Republic of China GB/T 12496.3-1999 and GB/T 12496.7-1999 respectively) were tested and calculated. The BET model (TristarII3020, Micromeritics, USA) was used to determine the specific surface area with the N_2 adsorption/desorption isotherm carrying out at 77.3K. SEM (SU8010, Hitachi, Japan) was employed for the surface morphology scanning. The chemical elements of the BCs were analyzed through XRF (ZSX PrimusII, Rigaku, Japan). Boric acid was used as the tabletting substrate, with its testing voltage and current being 50kV and 60mA respectively. XRD (X'Pert Powder, PANalytical, Netherlands) was used to investigate the crystallization of the BC samples, and the conditions were set as CuKα, 40kV, 40mA. The scanning peaks were collected in the range of 5~80°, then the analysis of the data was done through MDI Jade 6.0. According to the XRF test results, the main soluble alkali and alkaline-earth metals (K^+, Na^+, Ca^{2+}, Mg^{2+}) were measured through the following steps: (1) Accurate weighing of the BC sample at 1.00 g, which was then mixed with 20 mL deionized water. (2) Oscillation was done at 25°C and 210 rpm for 24 h, then filtered with a 0.25μm membrane filter. (3) Testing by Flame Atomic Absorption Spectrophotometer (FAAS, TAS-990, Persee, China), following the National Standards of People's Republic of China GB/T 11904-89 and GB/T 11905-89.

$$Yield(\%) = \frac{wheat\ straw\ weight}{biochar\ weight} \times 100\% \quad (2\text{-}1)$$

$$Net\ Yield(g/g) = \frac{yield \times (1 - ash\ content)}{1.0000} \quad (2\text{-}2)$$

2.3. Batch adsorption/desorption experiments

As Liu et al. [40] described, pores on the surface of biochar could be blocked by ash particles and dissolved alkalinity or other additional components that could affect the pH values of adsorbate solutions thus influence the Hg(II) removal efficiency. In this experiment, BCs were washed by deionized water until it turns liquid to neutral, then dried at 105°C for 12 h, in which were referred to WBC300, WBC400, and WBC600.

For the preparation of simulate mercury-containing wastewater with initial concentration of 2 mg/L, 0.3236 g $Hg(NO)_3$ was dissolved in 1 L deionized water, then diluted 100 times, and the background ion strength was 0.01 M $NaNO_3$. All the experiments were performed in triplicate, with the WBC dosage of 0.03 g per 50 mL Hg(II) solution in centrifuge tubes which were then oscillated at 25°C, 210 rpm for 24 h, and further filtered with a 0.25 μm membrane filter without special instructions. For mercury concentration testing, an Atomic Fluorescence Spectrometer (AFS, AFS-9700, Haiguang Instrument Co., Ltd, China) was used with the following conditions: negative pressure of photomultiplier tube being 300V, lamp current at 30mA, and carrier agent and reducing agent at 5% HNO and 10% KBH_4 respectively (followed by Environmental Protection Standards of the People's Republic of ChinaHJ694-2014).

2.3.1. Effects of pH

The adjustment of the pH ranges of solutions with 50mL simulated wastewater rated from 2.0 to 11.0 through the addition of 0.1 M HNO_3 and NaOH as per-required. The residual mercury concentration in the solutions was then tested by AFS after the adsorption reaction was conducted.

2.3.2. Isotherm studies

Different Hg(II) concentration solutions were obtained for WBCs adsorption isotherms (0.1, 0.5, 1, 2, 4, 6, 8 and 10 mg/L) at pH=6. Mercury removal rate η (%) and uptake capacity q_t (mg/g) of WBC300, WBC400, and WBC600 after adsorption equilibrium were calculated as equation 2-3 and 2-4 shows. Experimental data were then fitted to two empirical isotherm models (Langmuir and Freundlich) as equation 2-5, 2-6 and 2-7 shows.

$$\eta = \frac{C_0 - C_t}{C_o} \times 100\ \% \tag{2-3}$$

$$\mathrm{q_t} = \frac{\mathrm{C_0} - \mathrm{C_t}}{\mathrm{m}}\mathrm{V} \tag{2-4}$$

$$Langumuirequation\colon q_e = \frac{K_L q_m C_e}{1 + K_L C_e} \tag{2-5}$$

$$K_R = \frac{1}{1 + K_L C_0} \tag{2-6}$$

$$Freundlich\ equation\colon q_e = K_F {C_e}^{1/n} \tag{2-7}$$

Where C_0, C_t and C_e are the initial, t time and adsorption equilibrium concentration of simulate mercury-containing wastewater respectively (mg/L), m is WBC dosage (0.03 g), V is solution volume (50 mL), q_e is equilibrium adsorption capacity (mg/g), K_L is Langmuir constant (L/mg), q_m is maximum adsorption capacity(mg/g), K_R is a dimensionless parameter, K_F is Freundlich constant (L/g), $1/n$ is another dimensionless parameter.

2.3.3. Kinetic studies

A preparation of a constant Hg(II) concentration of 2 mg/L with pH=6 was reserved for the adsorption kinetics study. A conduction of an estimated test of the remaining Hg(II) concentration in equilibrium conditions at prescribe time intervals (1, 5, 10, 20, 30, 40, 60, 120, 180, 240, 480, 600, 720, 900 and 1440 min) was taken place and then fitted with pseudo first-order and pseudo second-order models (as equation 2-8, 2-9 shows).

$$Pseudo\ first-order\ equation\colon q_t = q_e[1 - \exp(-k_1 t)] \tag{2-8}$$

$$Pseudo\ second-order\ equation\colon q_t = \frac{k_2 {q_e}^2 t}{1 + k_2 q_e t} \tag{2-9}$$

Where q_e is equilibrium adsorption capacity (mg/g), q_t is adsorption capacity at t time (mg/g), K_1 and K_2 are rate constant for the pseudo first-order adsorption (1/min) and pseudo second-order adsorption (g/(mg·min)) respectively.

2.3.4. Static desorption experiments

Separating the WBC and solution after adsorption experiment (when WBC achieved adsorption equilibrium) with initial Hg(II) concentration of 2mg/L, then calculating the equilibrium adsorption capacity q_e (mg/g) by testing the remaining mercury concentration in the filtrate. The above WBC

samples were then added into three kinds of desorption solutions namely deionized water, 0.01 M HNO_3 and $NaNO_3$ at pH=6, and oscillated at 25°C, 210 rpm for 24 h. After the reaction and filtration, the desorption capacity q_d (mg/g) and desorption rate η (%) were analyzed as equation 2-10 and 2-11.

$$q_d = \frac{C_d}{m} V \tag{2-10}$$

$$\eta = \frac{q_d}{q_e} \times 100\% \tag{2-11}$$

Where C_d is equilibrium desorption capacity (mg/L), m is WBC dosage (0.03 g), V is solution volume (50 mL).

2.3.5. Adsorption in binary wastewater system

A batch concentrations of metallic ions Cd(II) and Pb(II) in the solution which ranged from 0.1 to 10 mg/L were found from their nitrates and coexisted with 2mg/L Hg(II) at pH=6 for the formation of a binary system respectively. One of the three WBC samples which had maximum adsorption efficiency was chosen to explore the capture capability of Hg(II) in the mixed simulate wastewater. Testing for Cd(II) and Pb(II) concentration followed by National Standards of People's Republic of China GB 7475-87.

2.4. Investigation of adsorption mechanism on mercury by wheat straw biochars

A investigation before and after adsorption equilibrium was done on the surface functional group variations of WBCs by FT-IR (Tensor27, Bruker, Germany). The samples were mixed with KBr powder and compressed tablet. The FT-IR was recorded with a 0.6 cm^{-1} resolution and 4000 to 600 cm^{-1} infrared domain. The pH value which is required to give zero net surface charge to make adsorbent become neither positively or negatively is designated as pH_{PZC} (point of zero charge).The pH_{PZC} of WBCs was determined as previous researches had reported [41, 42]. The concentration changes of the main soluble metallic ions K^+, Na^+, Ca^{2+}, and Mg^{2+} were measured before and after the adsorption equilibrium of 20 mg/L Hg(II) solution with pH=6, a WBC dosage of 0.3 g and the inability of setting the ion strength were obtained, the above steps of 2.2. (2) and (3) were then to be followed.

3. Results and discussion

3.1. Characterization of wheat straw biochars

Table 1 shows the yield, ash content, and pH of BCs which were pyrolyzed at 300°C, 400°C and 600°C. As seen, the ash content and pH values indicates an improvement as the pyrolysis temperature increased, making BC600 as high as 30.54% and 10.58 respectively due to the increased concentration of non-pyrolyzed inorganic elements in wheat straw. Nevertheless, low temperature biochar shows a higher yield because of the minimal condensation of aliphatic compounds and less loss of volatile gas [43].

Table 1. Yield, ash content, net yield and pH of BCs

Samples	Yield (%)	Ash Content (%)	Net Yield (g/g)	pH
BC300	51.62	18.17±0.76	0.42±0.00	7.55±0.36
BC400	37.25	21.77±0.80	0.29±0.00	8.54±0.16
BC600	34.03	30.54±1.22	0.24±0.00	10.58±0.41

Table 2. The textural parameters of BCs

Samples	Mass	S_{BET}	S_{BET} of Micropore	Micropore Volume	S_{BET} of Mesopore	Mesopore Volume	Total Pore Valume	Average Pore Size

	(g)	(m^2/g)	(m^2/g)	(cm^3/g)	(m^2/g)	(cm^3/g)	(cm^3/g)	(nm)
BC300	0.1705	2.77	—	—	1.00	0.0082	0.0083	17.13
BC400	0.1803	5.33	0.93	0.0003	2.34	0.0093	0.0167	12.87
BC600	0.1800	55.92	39.47	0.0184	7.38	0.0101	0.0320	6.09

Table 2 shows the textural parameters of BCs. Specifically, the S_{BET} had a rapid increase from BC400 (5.33 m^2/g) to BC600 (55.92 m^2/g), and BC600 had micropore development which could be verified by relatively high S_{BET} value in the micropore (39.47 m^2/g) and a low value of the average pore size (6.09 nm). The N_2 adsorption/desorption measurements are performed in Fig. 1. The Type Ⅱshape of the IUPAC classification was followed by these three plots. It also displayed an H4 hysteresis loop [44], which was related to the typical single to multi-layer adsorbing carbon materials. When $P/P_0$was in the lower pressure range of 0~0.3, BC600 expressed an anti-S type for the N_2 adsorption curve with a significant increase of adsorbance which indicates the microporous structure bearing a diameter of less than 2nm in the biochar. In addition, the occurrence of a multi-layer adsorption was in the high pressure range of 0.8~1.0, the first increase of N_2 adsorption capacity in BC300 and BC400 indicates the textural structure mainly consisted of mesopores bearing a diameter between 2~50nm, and macropores bearing a diameter larger than 50nm. The adsorption capacity of these three biochars satisfies BC600 > BC400 > BC300 when P/P_0 was close to 1, in which demonstrates increasing pyrolysis temperature provided positive benefits to the development of porosity and total pore volume [45, 46].

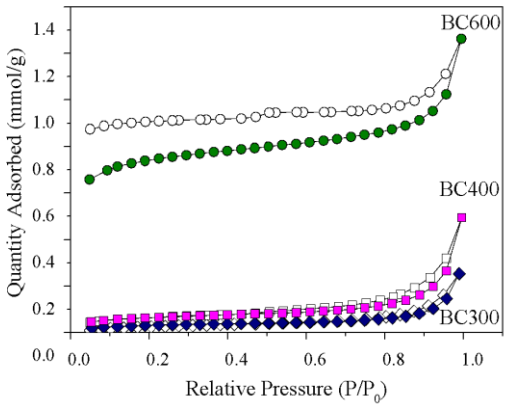

Fig. 1 N_2 adsorption/desorption isotherm plots for BCs

The morphology was visualized by means of SEM, it could be observed that the textural properties had visible changes with different charring temperatures (Fig. 2). The formation of a bundle-shaped tube on BC300 created uneven sized pores bearing a diameter range between 5~8 μm. On the other hand, the pores of BC400 were more well-distributed. Compared to low temperature biochars, BC600 possessed a neater tubular structure and thinner pore walls which led to bear a larger pore opening as high as 15~18 μm. Seen from the enlargement of c2, c3 shows smaller pores generated that consistent with previous textural parameters results. Tiny carbon slices or ash particles were clearly adhered to the surface of the biochar inhomogeneously which could be removed by deionized water or acid solutions [47, 48]. In general, the carbonized structure of biochars showed the potential for contaminants removal.

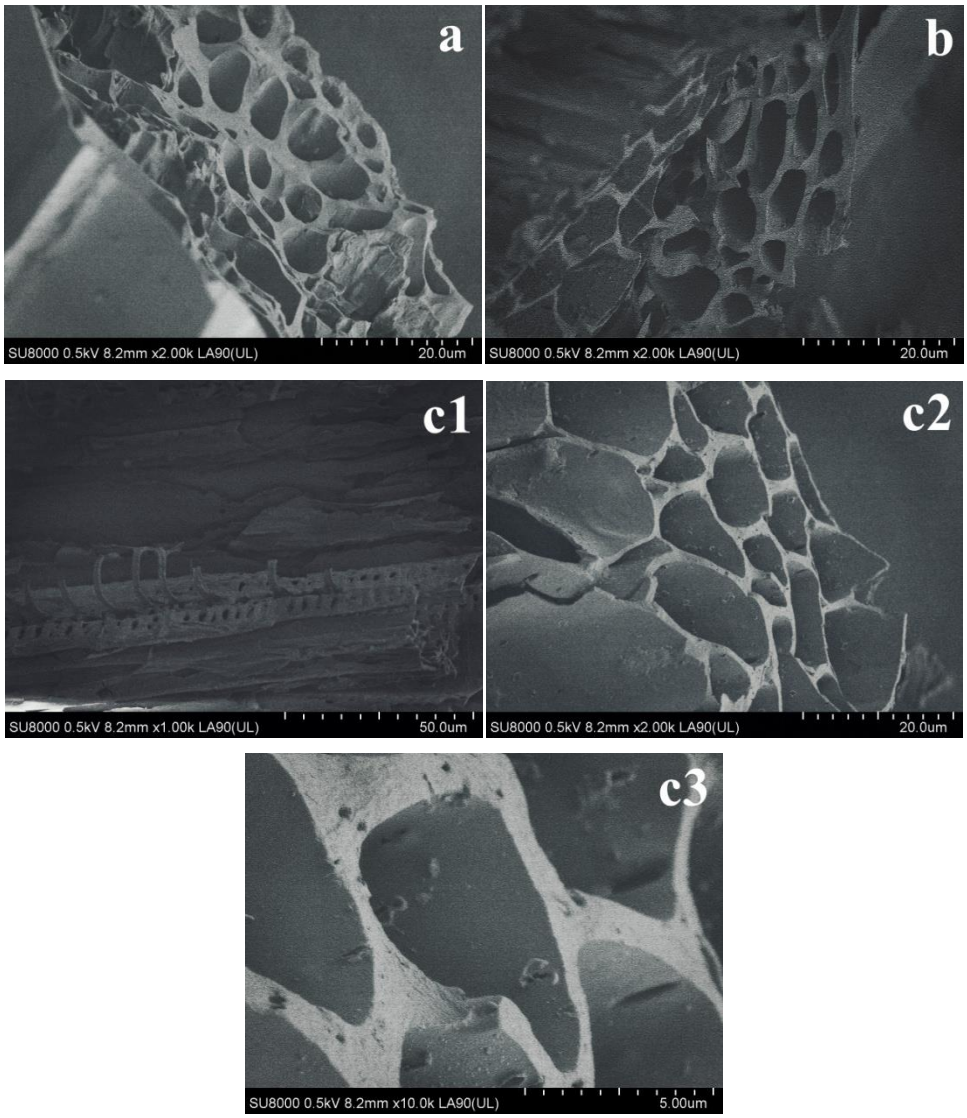

Fig. 2 SEM images of BCs

(a) BC300×2.00k, (b) BC400×2.00k, (c1, c2, c3) BC600×1.00k, ×2.00k, ×10.0k

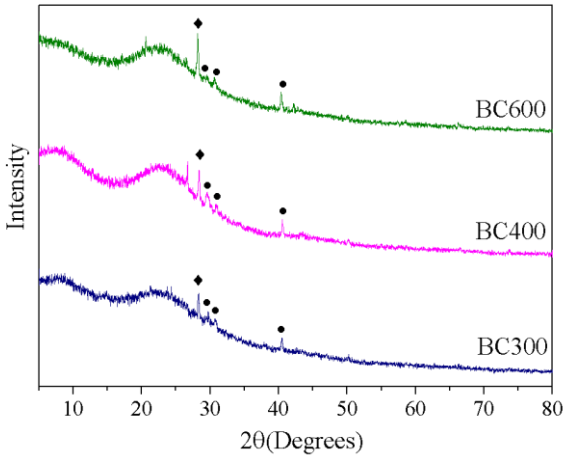

Fig. 3 The X-ray diffraction spectrafor BCs (◆silica, SiO_2 ●potassium sulfate, K_2SO_4)

The relative inorganic element and main water-soluble cation contents are shown in Table 3 and 4.

As can be seen, K and Ca account for the largest proportions of metallic elements in BCs (52.02, 53.47, 48.04 %wt for BC300, BC400, and BC600, respectively), while Si accounts for the highest amount of the non-metallic elements (36.43, 35.51, 40.19 %wt for BC300, BC400, and BC600, respectively) due to its strong ability to absorb nutrients like silicon in soil for crop growth and yield improvement, also it would not loss during pyrolysis process as temperature increased [49]. It should be noted that the concentrations of water-soluble K^+, Na^+, Ca^{2+}, and Mg^{2+} increased as pyrolysis temperature enhanced. Among them, K^+ occupied the highest proportion which echoed XRF results. These cations mainly came from alkali dissolutions and likely competed with heavy metals for the negatively charged points on biochar surface resulting to a decreased adsorption efficiency. Based on these elemental determinations, XRD analysis was performed (Fig. 3). Results shows that there were no obvious crystal substances presented in this kind of wheat straw biochar and only silica (SiO_2, diffraction peaks at 28.14°) and potassium sulfate (K_2SO_4, diffraction peaks at 29.55, 30.39 and 40.53°) were found in their subcrystalline forms, with more prominent crystallization and higher diffraction peaks of silica at increased pyrolysis temperatures. This was analogous to the changes in the XRD spectra of a corn straw biochar, as reported by Yuan et al. [50], no crystals were observed at 300°C biochar, further the presence of calcite ($CaCO_3$), dolomite ($CaMg(CO_3)_2$), and sylvite (KCl) peaked at 3.03, 2.90 and 3.15 Å respectively at a pyrolysis temperature of 500 °C, which were confirmed by several more peaks forming at 700°C. Thus, it can be concluded that the crystalline mineral components of such straw biochars are not abundant.

Table 3 The XRF results of BCs

Elements	The relative content (%wt)		
	BC300	BC400	BC600
K	39.27	38.98	36.96
Ca	12.75	14.49	11.08
Mg	1.00	1.17	1.26
Na	0.09	0.06	0.10
Fe	0.53	0.65	0.67
Mn	0.21	0.25	0.24
Al	0.23	0.23	0.31
Zn	N.A.	0.12	0.16
Si	36.43	35.51	40.19
Cl	4.89	3.78	3.80
S	2.73	2.35	2.23
P	1.87	2.41	3.00

Table 4 Content of water-soluble cations of BCs

Cations	Concentration (mg/g)		
	BC300	BC400	BC600
K^+	14.08±0.29	17.85±0.12	34.03±3.43
Na^+	0.28±0.06	0.30±0.07	0.30±0.06
Ca^{2+}	0.47±0.06	0.51±0.07	0.79±0.07
Mg^{2+}	0.15±0.03	0.10±0.02	0.27±0.07

3.2. Effects of initial pH on Hg(II) removal efficiency

The interaction between Hg(II) ions and biochar depends on the pH of the solution as it affects metal speciation, surface charges and mineral components dissolution of adsorbent. Since pH is an important

parameter, the biochars previously washed by deionized water (referred as WBCs) were underwent batch experiments to avoid affecting the alkalinity on initial pH. The present study demonstrates the variations in the removal efficiency of Hg(II) at a wide range pH values (Fig. 4).

Under different pH conditions, the Hg(II) adsorption efficiencies of WBCs at three pyrolysis temperatures were almost the same. An increase in the removal efficiency of Hg(II) was directly proportional to the pH values within a range of 2.0~6.0, where the maximum rate of increase occurred at 2.0 to 3.0. It was further verified that $Hg(OH)^+$ and Hg^{2+} were the dominant species (accounting for more than 70% of mercury in solution) at pH 2.0~3.0 [2], while the surface of WBCs was protonated. At this point, there was a repulsive force between the WBCs and mercury-containing cations, which further decreased mercurial adsorption on the surface and pores of biochar. On the other hand, alkali and alkaline earth metals (K^+, Na^+, Ca^{2+}, Mg^{2+}, etc.) dissolved in strong acid solutions with large numbers of H^+, caused competition in the adsorption with mercury-containing cations and resulting in lower removal efficiency. Then, with a continuous increase in pH, the removal efficiency of WBC300 and WBC400 had reached a plateau at a pH range of 6.0~8.0, further decreased as pH went up to 11.0, whereas the removal efficiency of WBC600 maintained a downward trend from pH 6.0 to 11.0. Hereinto, the maximum removal efficiency obtained at pH 6 was 97.1%, 94.3% and 90.2% for WBC300, WBC400, and WBC600, respectively. In neutral and alkalescency environments, competitive adsorption was less prominent due to the decrease in metallic cation concentration and deprotonation of the biochar surface as pH gradually rising up [51]. When pH changed to strong alkaline, $Hg(OH)_2$ was formed via the increased concentration of OH^- and the hydrolysis of Hg(II), which reduced the freedom degree of mercury, making it unfavorable to adsorption, but the result was much desired than strong acid condition might due to the $Hg(OH)_2$ precipitation. To consolidate the above analysis, the subsequent experiments were all carried out at pH 6.0, which was proposed by previous researches that highest Hg(II) adsorption capacity occurred at a pH range of 4~6 [34].

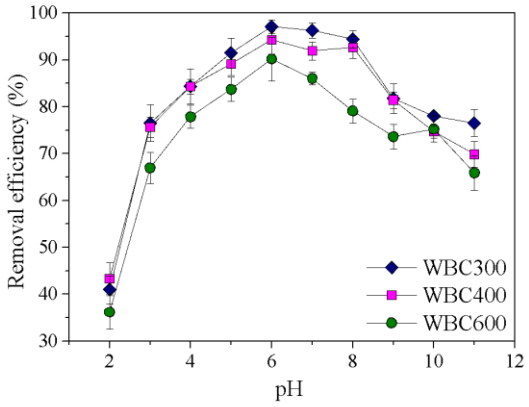

Fig. 4 Effects of initial pH on Hg(II) removal efficiency

3.3. Adsorption isotherms

Adsorption isotherms provide a means of evaluating the maximum adsorption capacities of adsorbent and applicability of a complete adsorption operation through a proceeding until the remaining adsorbate existing in the equilibrium solution system. Moreover, the fitting of adsorption isotherm models reflects the interaction mechanisms between the adsorbent and the adsorbate [52].

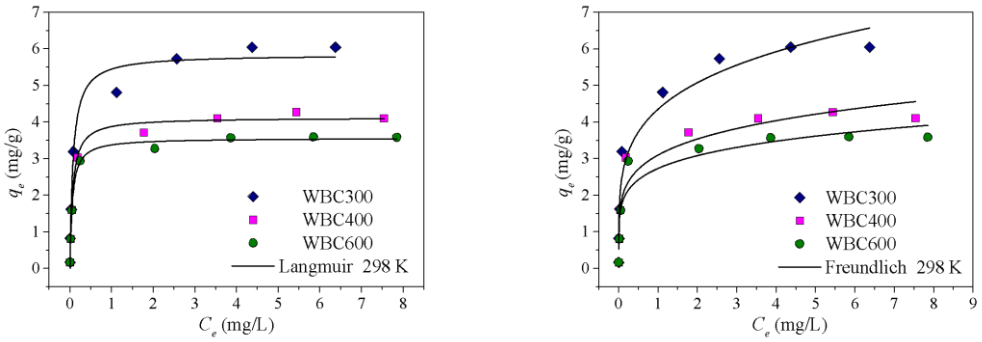

Fig. 5 Non-linear fits of Langmuir and Freundlich isotherm models of Hg(II)adsorption on WBCs

The non-linear fits to the Langmuir and Freundlich empirical isotherms of experimental data are depicted in Fig. 5, and the isothermal parameters are listed in Table 5. The correlation coefficient value R^2 estimates the fitness to isotherm models, as observed, the R^2 of Langmuir models are all greater than that of Freundlich models, which presented similar results to that of Hg(II) removal using activated carbon impregnated with humic acid [53], indicating that the Langmuir isotherm model was more suitable for describing the adsorption process of Hg(II) onto WBCs, and that the adsorption process occurred on a homogeneous surface of biochar. As per theoretical foundation, the Langmuir isotherm model assumes that adsorbent surface is a homogeneous monolayer with a certain amount of adsorption active sites, and each adsorbate molecule bonds to one site until all of them are occupied, which then saturates the adsorbate and allows to reach its maximum adsorption capacity (q_m) [54]. The theoretical q_m determined from Langmuir model were 5.85, 4.13 and 3.56 mg/g for WBC300, WBC400, and WBC600 respectively, which were close to the experimental values 6.05, 4.27, 3.59 mg/g with standard deviation were 14.14, 9.90 and 2.12%, respectively, showing that q_m are ranked as WBC300 > WBC400 > WBC600. In addition, the dimensionless parameter K_R indicates the type and favorability of isotherms, dividing it into unfavorable ($K_R > 1$), linear ($K_R = 1$), favorable ($0 < K_R < 1$) and irreversible ($K_R = 0$) [55]. Seen from Table 5, K_R are all within the range of 0~1, implying a favorable adsorption of Hg(II) on WBCs. It is worth to be mentioned that the higher the initial Hg(II) concentration, the smaller the K_R value, and the more favorable it would be to the adsorption process. The analogical conclusion could be derived from Freundlich parameter *1/n*, where a value between 0 to 0.5 manifests that the Hg(II) was facile to be adsorbed to WBCs (*1/n* = 0.1740~0.2225 for WBCs) [51].

Table 5 Adsorption isotherm parameters for Hg(II)removal on WBCs at 298K

Samples	Langmuir isotherm model					Freundlich isotherm model		
	$q_{m\,exp}$ (mg/g)	$q_{m\,the}$ (mg/g)	K_L (L/mg)	K_R	R^2	K_F (L/g)	*1/n*	R^2
WBC300	6.05±0.24	5.85	13.66	0.0073~0.4227	0.9782	4.35	0.2225	0.9543
WBC400	4.27±0.10	4.13	15.67	0.0063~0.3895	0.9909	3.10	0.1915	0.9090
WBC600	3.59±0.30	3.56	18.12	0.0055~0.3556	0.9932	2.73	0.1740	0.8912

"exp" is experimental value, "*the*" is theoretical value.

3.4. Adsorption kinetics

The adsorption of Hg(II) onto WBCs can be divided into two stages: (1) A rapid stage took place within the first 10 minutes where the removal rate and adsorption capacity reached its largest increase, (2) After that, slow stage showed a gentle adsorption increase rate until equilibrium was reached in 240 min

for WBC300 and WBC400, 360min for WBC600. Fig. 6 depicts the non-linear fits of pseudo first-order and pseudo second-order empirical models, and the kinetics parameters are listed in Table 6.

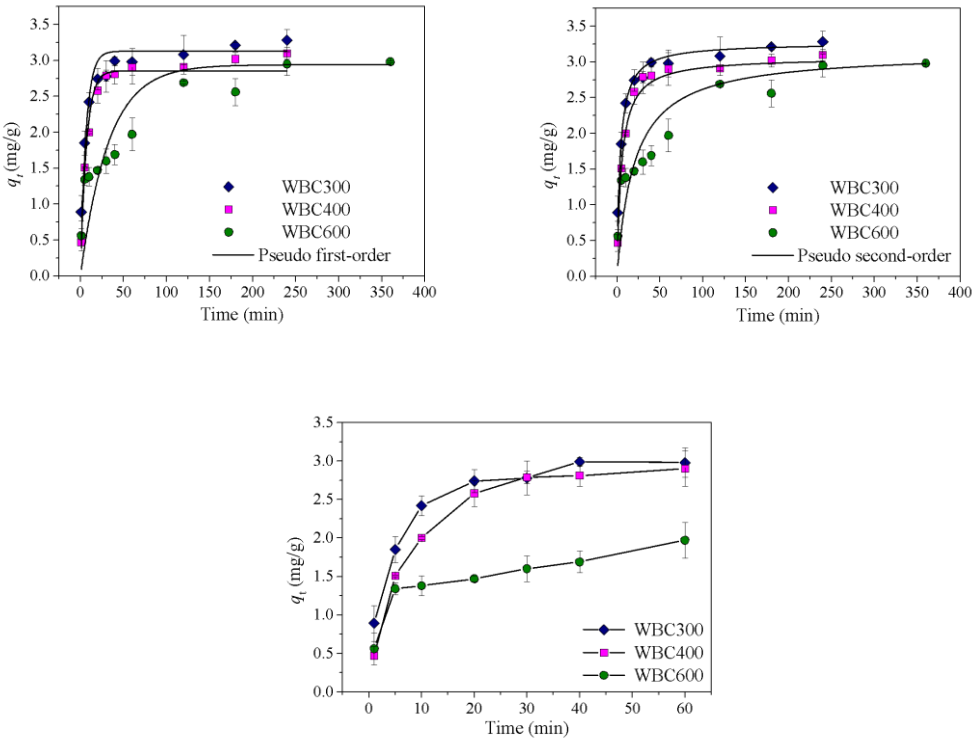

Fig. 6 Non-linear fits of pseudo first-order, pseudo second-order kinetics models of Hg(II)adsorption on WBCs and partial section of adsorption kinetics curve

As shown below, the pseudo second-order kinetic model presented a higher R^2 for the three biochars, and the theoretical equilibrium capacity ($q_{e\ the}$ were 3.27, 3.07 and 3.14 mg/g for WBC300, WBC400, and WBC600, respectively) was close to the experimental value ($q_{e\ exp}$ were 3.28, 3.10, 2.98 mg/g for WBC300, WBC400, and WBC600, respectively), with corresponding standard deviations of 0.71%, 2.12% and 11.31%. This implies that the adsorption of Hg(II) by WBCs is not only determined by a single factor, but by a variety of mechanisms, and that the main rate determining step was controlled by chemical adsorption, involving surface adsorption and valence forces such as ion or electron exchange [55, 56]. Additionally, Rao et al. [57] achieved the similar result with our kinetics study. As for K_2 values of these three biochar are ranked in the order WBC300 ≈ WBC400 > WBC600, indicating that the adsorption rates of first two WBCs were greater than that of WBC600 and explains why the former reached adsorption equilibrium more faster, which is consistent with the practical situation.

Table 6 Adsorption kinetics parameters for Hg(II) removal on WBCs

Samples	q_{eexp} (mg/g)	Pseudo first-order kinetic model			Pseudosecond-order kinetic model		
		K_1 (min^{-1})	$q_{e\ the}$ (mg/g)	R^2	K_2 ($gmg^{-1}min^{-1}$)	q_{ethe} (mg/g)	R^2
WBC300	3.28±0.15	0.15	3.13	0.8772	0.08	3.27	0.9894
WBC400	3.10±0.08	0.14	2.86	0.9601	0.06	3.07	0.9964
WBC600	2.98±0.01	0.03	2.94	0.8557	0.02	3.14	0.9421

3.5. Desorption of Hg(II) in different agents

Desorption study provides a method to explore the usability of adsorbent and further investigating the adsorption mechanism. Generally, inorganic acid agents desorb the heavy metal ions by increasing the concentration of H^+ which could combine with the surface functional groups of adsorbents. Inorganic salt agents have a similar desorption mechanism with inorganic acids that large amounts of cations are introduced into solution, which seize the adsorption sites by exchanging ions with Hg(II). Although deionized water is used as a low-cost desorbent agent, it can only separate Hg(II) adsorbed by physical forces such as electrostatic interaction and Van-der Waals forces between molecules, but has little effect on Hg(II) adsorbed chemically. It can be seen from Fig. 7 that the desorption efficiencies of three desorbing agents on WBC300 and WBC400 are ranked as $HNO_3 > NaNO_3 > H_2O$. Acidic solutions were proved to be the most efficient in the desorption of Hg(II) from biochars with a desorption capacity of 1.03, 1.03 mg/g and a desorption rate of 30.9, 31.5% for WBC300 and WBC400 respectively. This indicates that the mechanisms of Hg(II) adsorption onto biochar might be through complexation reaction with its functional groups. In contrast to the desorption effect of the three biochars in the similar agent, it is found that the desorption capacities and rates of WBC600 in H_2O and $NaNO_3$ were higher than that of low temperature pyrolysis biochars, with values up to 0.84 mg/g and 26.8% respectively, but was slightly lower in HNO_3. It can be speculated that the WBC600 did not mainly rely on the complexation reactions to adsorb Hg(II), and that electrostatic or ion exchange reactions might be the dominating mechanism. In addition, the overall desorption rates of three agents were less than 50%, which due to the limited concentration of desorption agents [58].

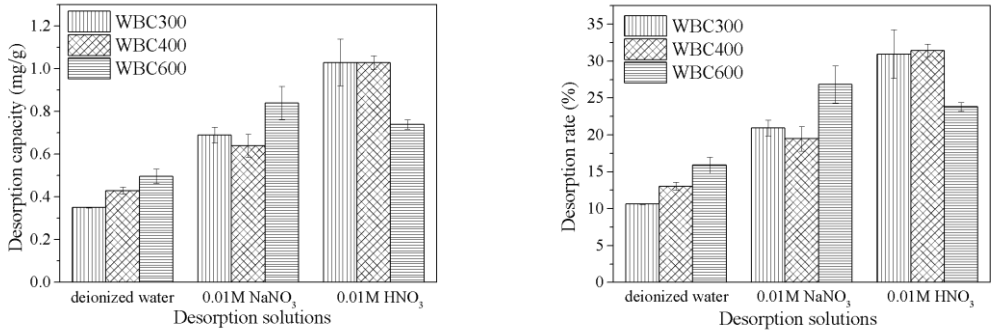

Fig. 7 Effect of different desorption solutions to WBCs

3.6. Competitive adsorption of Hg(II) in binary systems

As mentioned above, the WBC300 had a relatively larger adsorption capacity among the three biochars. In this part, WBC300 was used to probe the competitive adsorption efficiency of Hg(II) in Hg-Cd and Hg-Pb binary systems. Fig.8 shows that with an increase in the initial concentration of Cd(II), the removal rate of Hg(II) was stable at about 95%, while the removal efficiency of Cd(II) was more than 99% with an initial concentration from 0.1~5 mg/L, and when further improved to 10 mg/L, the removal efficiency reduced to 70.9%, with an increasing adsorption capacity of Cd(II) onto WBC300 which reached 11.81 mg/g. However, the WBC300 in Hg-Pb binary system shows a rather different result. For a high initial concentration of Pb(II) at 10 mg/L, the removal efficiency of Pb(II) was only 73.0% with adsorption capacity was 12.26 mg/g, Hg(II) removal rate suddenly decreased to 77.2% which indicates that there was a competition adsorption between Pb(II) and Hg(II), but no obvious impact between Cd(II) and Hg(II).

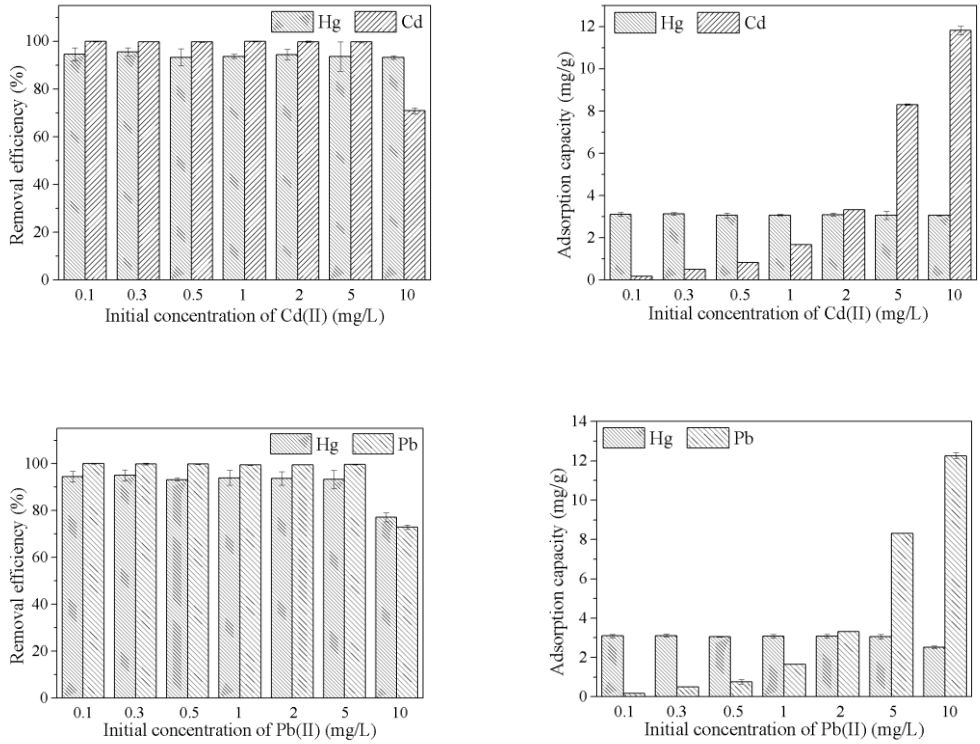

Fig. 8 Removal efficiency and adsorption capacity of WBC300 in binary systems

In order to further understand the dynamics of wheat straw biochar adsorption, q_e'/q_e ratios were utilized for calculations (q_e' and q_e are equilibrium uptake capacities in binary and single systems respectively), when $q_e'/q_e > 1$ indicates that the equilibrium adsorption capacity of heavy metal ions in the binary system is larger than that of the single system, means the coexisting ions have synergistic effect on adsorption; on the contrary, $q_e'/q_e < 1$ means antagonism effect between coexisting heavy metal ions; $q_e'/q_e = 1$ means coexisting ions have noninteraction to adsorbent compared with single systems [59]. Hg(II), Cd(II) and Pb(II) were the main adsorbates ordinally and their ratio values are shown in Table 7. The q_e'/q_e for Hg-Pb and Pb-Hg binary systems were 0.81 and 0.97 respectively, which implies that antagonistic effect influenced the adsorption reaction in binary systems. Furthermore, the effect of Pb(II) on Hg(II) was higher than that of Hg(II) on Pb(II). The reason for this phenomenon might be explained by Pb(II) and Hg(II) having partially similar adsorption sites on the biochar, and Hg(II) was uncompetitive for the active sites when the initial concentration of Pb(II) was much higher than Hg(II). Moreover, Pb(II) has two possible coordination numbers (4, 6), as well as lager atomic number and electronegativity than Hg(II). All these factors favor the adsorption of Pb(II) by bio-adsorbent [60].

Table 7 Equilibrium adsorption capacity in binary systems

Main adsorbates	Initial concentration of Cd(II)/Pb(II) (mg/L)						
	0.1	0.3	0.5	1	2	5	10
Hg(II)				q_e'/q_e			
Hg-Cd	0.99	1.00	0.98	0.98	0.99	0.98	0.98
Hg-Pb	0.99	1.00	0.98	0.99	0.99	0.98	0.81
Cd(II)				q_e'/q_e			
Cd-Hg	1.01	1.01	1.00	1.00	1.00	1.00	1.00
Pb(II)				q_e'/q_e			

Pb-Hg	1.00	1.00	1.03	1.00	1.00	1.00	0.97

The concentration of Hg(II) in all systems were 2 mg/L.

3.7. Adsorption mechanism exploration

The three biochars all had high pH_{pzc} (7.18, 7.23 and 7.58 for WBC300, WBC400 and WBC600 respectively, as shown in Fig. 9), that were a little lower than bagasse and hickory chip biochars, as well as a commercial activated carbon (8.5~9.9) without deionized water washing [36]. By observing that the equilibrium pH of both WBC300 and WBC400 was prominently lower than the initial pH in alkaline range, it can be proven that the acidic functional groups were located on the surface of biochars. It was previously mentioned that the optimum adsorption pH was 6.0, which was lower than the pH_{pzc}. This, therefore, implies that the adsorption mechanism through physical forces such as electrostatic interaction was inessential because of the protonation on biochar surface at that certain pH.

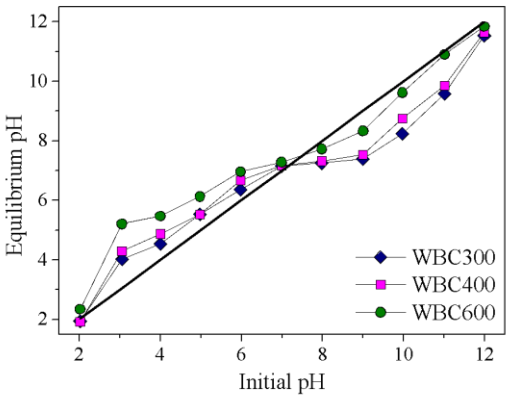

Fig. 9 Point of zero charge (pH_{PZC}) curves of WBCs

For chemical mechanism, FT-IR spectra of WBCs before and after adsorption process are presented in Fig. 10. The three biochars all had infrared absorption peaks at 1600 cm^{-1} and 1702 cm^{-1} caused by the stretching vibration bands of C=C and C=O, which could determine the presence of carboxyl combined with another stretching vibration band of O-H at 3430 cm^{-1}. Moreover, the peak that appeared at 1091 cm^{-1} was considered to be the C-O stretching vibration, then the alcoholic hydroxyl and phenolic hydroxyl could be affirmed by associating with O-H [61]. As shown in Fig. 10, the carboxyl, alcoholic and phenolic hydroxyl were obtained on the surface of WBC300 and WBC400, however, the absorption peaks weakened at 3430 cm^{-1}, 1702 cm^{-1}, 1600 cm^{-1}, and 1091 cm^{-1} after the adsorption of Hg(II) that indicated the reduction in the amount of above oxygen-containing functional groups and further demonstrating their complexations with Hg(II), which was evident in WBC300 (as 3-1 and 3-2 proposed). The absorption peaks recorded at 2925 cm^{-1}, 1378 cm^{-1}, and 798 cm^{-1} were generally considered to be the stretching vibrations of hydrocarbon C-H and the scissor bending vibration of $-CH_2-$ [61] It is further shown that with an increase in the biochar pyrolysis temperature, comes a decrease in absorption peaks, indicating the gradual aromatization of biochars. These three weaker peaks showed no significant changes after the adsorption of Hg(II), which means they had no association with the mechanism of Hg(II) removal. The functional groups in high temperature biochar WBC600 were much less than that of WBC300 and WBC400, however, only the peaks recorded at 1600 cm^{-1} and 1091 cm^{-1} were weakened after Hg(II) adsorption, indicating that the complexations of Hg(II) with the oxygen-containing functional groups onto WBC600 were unconspicuous.

$$—COOH + Hg^{2+} \rightarrow —COOHg^{+} + H^{+} \quad (3\text{-}1)$$

$$—OH + Hg^{2+} \rightarrow —OHg^{+} + H^{+} \quad (3\text{-}2)$$

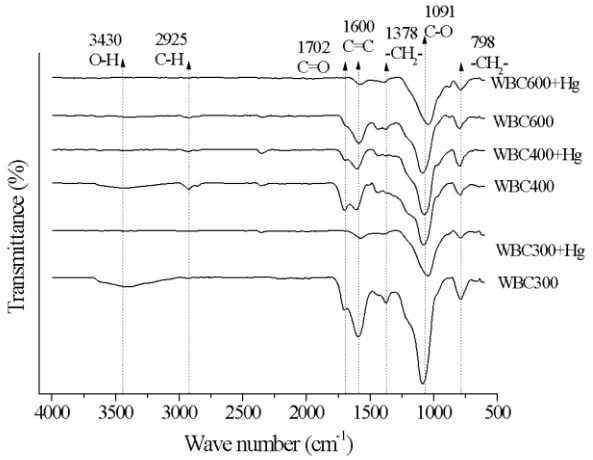

Fig. 10 FT-IR spectra of WBCs before and after adsorption processing

Additionally, the results of water-soluble cation contents show that the release of K^+ and Ca^{2+} was distinct (Table 8), and the released quantity of WBC600 was almost twice greater than that of WBC300. Similar results were reported in Hg(II) adsorption by activated sludge biomass where ion exchange processes were contained in mechanism exploration [62], and was especially obvious in high temperature biochars.

Table 8 Content of water-soluble cations of WBCs before and after adsorption

		Concentration of cations (mg/g)			
		K^+	Na^+	Ca^{2+}	Mg^{2+}
Before adsorption	WBC300	2.70±0.06	0.04±0.02	0.25±0.02	0.05±0.01
	WBC400	2.85±0.12	0.04±0.02	0.24±0.02	0.04±0.00
	WBC600	2.52±0.38	0.05±0.00	0.25±0.08	0.05±0.01
After adsorption	WBC300	11.29±0.20	0.09±0.02	6.49±0.38	1.45±0.30
	WBC400	14.47±0.25	0.09±0.03	8.77±0.60	2.21±0.45
	WBC600	18.79±0.39	0.19±0.03	11.67±0.82	2.37±0.44
Net release quantity	WBC300	8.59±0.02	0.04±0.01	6.25±0.46	1.41±0.21
	WBC400	11.62±0.06	0.04±0.00	8.53±0.35	2.17±0.12
	WBC600	16.28±0.15	0.14±0.00	11.42±0.07	2.31±0.08

4. Conclusion

In this study, a wheat straw biochar was obtained via slow pyrolysis at three different temperatures (300°C, 400°C and 600°C) and was used as an adsorbent for the removal of Hg(II) from simulated wastewater. The physical and chemical characterization of biochar was done through a series of procedures including BET method, SEM, XRF, XRD, and FT-IR, while soluble metal testing was done mainly through FAAS. In order to prevent the effects of varying pH to soluble compounds during the adsorption and desorption processes, washed biochars were used in the reaction which included WBC300, WBC400 and WBC600. Experimental results showed that the three biochars all reached maximum Hg(II) removal efficiency at a pH solution of 6. The adsorption isotherm data was well fitted to the Langmuir model ($R_2 > 0.9782$), and the maximum laboratorial adsorbing capacities were recorded at 6.05, 4.27, and 3.59 mg/g for WBC300, WBC400, and WBC600, respectively. The adsorption kinetics data was fitted using a pseudo second-order model ($R_2 > 0.9421$). In addition, nitric acid exhibited a

relatively greater effect on Hg(II) desorption from WBC300 and WBC400 compared to WBC600, which indicated that a complexation with functional groups was involved in the adsorption mechanism. Interestingly, Pb(II) competed with Hg(II) in its adsorption sites on WBC300 when presented in binary system, however, Cd(II) had shown no impact on Hg(II) adsorption. It was summarized from the adsorption mechanism that low temperature biochars (WBC300 and WBC400) adsorbed Hg(II) mainly relied on complexation reactions with carboxyl, alcoholic and phenolic hydroxyl functional groups, while high temperature biochars (WBC600) mainly relied on ion exchange processes for Hg(II) adsorption, presenting different adsorption mechanism.

Finally, all above results demonstrates the efficiency of sustainable, renewable, and inexpensive biochar as a potent adsorbent for mercury removal, meanwhile it makes use of an environmentally-friendly adsorption mechanism without causing secondary pollution. The high adsorption efficiency in binary systems also provided a novel method for mixed heavy metal wastewater treatment under the premise of using less amounts of adsorbent.

Acknowledgments: This research was supported by Fuling Shale Gas Environmental Exploration Technology of National Science and Technology Special Project (Grant No.:2016ZX05060).

References

[1] Tan G, Sun W, Xu Y, Wang H, Xu N. Sorption of mercury (II) and atrazine by biochar, modified

biochars and biochar based activated carbon in aqueous solution. Bioresource technology. 2016;211:727-35.
[2] Dong X, Ma LQ, Zhu Y, Li Y, Gu B. Mechanistic investigation of mercury sorption by Brazilian pepper biochars of different pyrolytic temperatures based on X-ray photoelectron spectroscopy and flow calorimetry. Environ Sci Technol. 2013;47:12156-64.
[3] Boutsika LG, Karapanagioti HK, Manariotis ID. Aqueous Mercury Sorption by Biochar from Malt Spent Rootlets. Water, Air, & Soil Pollution. 2013;225.
[4] Yang J, Zhao Y, Ma S, Zhu B, Zhang J, Zheng C. Mercury Removal by Magnetic Biochar Derived from Simultaneous Activation and Magnetization of Sawdust. Environ Sci Technol. 2016;50:12040-7.
[5] Mahmoud ME, Ahmed SB, Osman MM, Abdel-Fattah TM. A novel composite of nanomagnetite-immobilized-baker's yeast on the surface of activated carbon for magnetic solid phase extraction of Hg(II). Fuel. 2015;139:614-21.
[6] Feng X, Li P, Qiu G, Wang S, Li G, Shang L, et al. Human Exposure To Methylmercury through Rice Intake in Mercury Mining Areas, Guizhou Province, China. Environmental Science & Technology. 2008;42:326-32.
[7] Mashhadi S, Sohrabi R, Javadian H, Ghasemi M, Tyagi I, Agarwal S, et al. Rapid removal of Hg (II) from aqueous solution by rice straw activated carbon prepared by microwave-assisted H2SO4 activation: Kinetic, isotherm and thermodynamic studies. Journal of Molecular Liquids. 2016;215:144-53.
[8] Lin Y, Wang S, Steindal EH, Wang Z, Braaten HF, Wu Q, et al. A Holistic Perspective Is Needed To Ensure Success of Minamata Convention on Mercury. Environ Sci Technol. 2017;51:1070-1.
[9] Han DS, Orillano M, Khodary A, Duan Y, Batchelor B, Abdel-Wahab A. Reactive iron sulfide (FeS)-supported ultrafiltration for removal of mercury (Hg(II)) from water. Water research. 2014;53:310-21.
[10] Richard JH, Bischoff C, Ahrens CG, Biester H. Mercury (II) reduction and co-precipitation of metallic mercury on hydrous ferric oxide in contaminated groundwater. The Science of the total environment. 2016;539:36-44.
[11] Nanseu-Njiki CP, Tchamango SR, Ngom PC, Darchen A, Ngameni E. Mercury(II) removal from water by electrocoagulation using aluminium and iron electrodes. Journal of hazardous materials. 2009;168:1430-6.
[12] Vasudevan S, Lakshmi J, Sozhan G. Optimization of electrocoagulation process for the simultaneous removal of mercury, lead, and nickel from contaminated water. Environmental Science and Pollution Research. 2012;19:2734-44.
[13] Siva S, Sudharsan S, Sayee Kannan R. Synthesis, characterization and ion-exchange properties of novel hybrid polymer nanocomposites for selective and effective mercury(ii) removal. RSC Adv. 2015;5:79665-78.
[14] Sinyakova MA, Semenova EA, Gamuletskaya OA. Ion exchange of copper(II), lanthanum(III), thallium(I), and mercury(II) on the "polysurmin" substance. Russian Journal of General Chemistry. 2014;84:2516-20.
[15] Ernesto Amabilis-Sosa L, Siebe C, Moeller-Chavez G, del Carmen Duran-Dominguez-De-Bazua M. Removal of mercury by Phragmites australis used as biological barrier in constructed wetlans inoculated with heavy metal-tolerant strains. REVISTA INTERNACIONAL DE CONTAMINACION AMBIENTAL. 2016;32:47-53.
[16] Giovanella P, Cabral L, Bento FM, Gianello C, Camargo FA. Mercury (II) removal by resistant bacterial isolates and mercuric (II) reductase activity in a new strain of Pseudomonas sp. B50A. New

biotechnology. 2016;33:216-23.
[17] Lee S-J, Park JH, Ahn Y-T, Chung JW. Comparison of Heavy Metal Adsorption by Peat Moss and Peat Moss-Derived Biochar Produced Under Different Carbonization Conditions. Water, Air, & Soil Pollution. 2015;226.
[18] López-Muñoz M-J, Arencibia A, Cerro L, Pascual R, Melgar Á. Adsorption of Hg(II) from aqueous solutions using TiO 2 and titanate nanotube adsorbents. Applied Surface Science. 2016;367:91-100.
[19] Cui L, Wang Y, Gao L, Hu L, Yan L, Wei Q, et al. EDTA functionalized magnetic graphene oxide for removal of Pb(II), Hg(II) and Cu(II) in water treatment: Adsorption mechanism and separation property. Chemical Engineering Journal. 2015;281:1-10.
[20] Wang Z, Xu J, Hu Y, Zhao H, Zhou J, Liu Y, et al. Functional nanomaterials: Study on aqueous Hg(II) adsorption by magnetic Fe3O4@SiO2-SH nanoparticles. Journal of the Taiwan Institute of Chemical Engineers. 2016;60:394-402.
[21] Tran L, Wu P, Zhu Y, Yang L, Zhu N. Highly enhanced adsorption for the removal of Hg(II) from aqueous solution by Mercaptoethylamine/Mercaptopropyltrimethoxysilane functionalized vermiculites. Journal of colloid and interface science. 2015;445:348-56.
[22] Yao X, Wang H, Ma Z, Liu M, Zhao X, Jia D. Adsorption of Hg(II) from aqueous solution using thiourea functionalized chelating fiber. Chinese Journal of Chemical Engineering. 2016;24:1344-52.
[23] Saleh TA. Isotherm, kinetic, and thermodynamic studies on Hg(II) adsorption from aqueous solution by silica- multiwall carbon nanotubes. Environmental science and pollution research international. 2015;22:16721-31.
[24] Gupta A, Vidyarthi SR, Sankararamakrishnan N. Enhanced sorption of mercury from compact fluorescent bulbs and contaminated water streams using functionalized multiwalled carbon nanotubes. Journal of hazardous materials. 2014;274:132-44.
[25] Budinova T, Petrov N, Parra J, Baloutzov V. Use of an activated carbon from antibiotic waste for the removal of Hg(II) from aqueous solution. Journal of environmental management. 2008;88:165-72.
[26] Fan L, Ling L, Wang B, Zhang R. The adsorption of mercury species and catalytic oxidation of Hg0 on the metal-loaded activated carbon. Applied Catalysis A: General. 2016;520:13-23.
[27] Li G, Wang S, Wu Q, Wang F, Shen B. Mercury sorption study of halides modified bio-chars derived from cotton straw. Chemical Engineering Journal. 2016;302:305-13.
[28] Ahmad M, Rajapaksha AU, Lim JE, Zhang M, Bolan N, Mohan D, et al. Biochar as a sorbent for contaminant management in soil and water: A review. Chemosphere. 2014;99:19-33.
[29] Keiluweit M, Nico PS, Johnson MG, Kleber M. Dynamic molecular structure of plant biomass-derived black carbon (biochar). Environmental Science & Technology. 2010;44:1247-53.
[30] Hwang H, Oh S, Cho T-S, Choi I-G, Choi JW. Fast pyrolysis of potassium impregnated poplar wood and characterization of its influence on the formation as well as properties of pyrolytic products. Bioresource technology. 2013;150:359-66.
[31] Jindo K, Suto K, Matsumoto K, García C, Sonoki T, Sanchez-Monedero MA. Chemical and biochemical characterisation of biochar-blended composts prepared from poultry manure. Bioresource technology. 2012;110:396-404.
[32] Manariotis ID, Fotopoulou KN, Karapanagioti HK. Preparation and Characterization of Biochar Sorbents Produced from Malt Spent Rootlets. Industrial & Engineering Chemistry Research. 2015;54:9577-84.
[33] Xue L, Gao B, Wan Y, Fang J, Wang S, Li Y, et al. High efficiency and selectivity of MgFe-LDH modified wheat-straw biochar in the removal of nitrate from aqueous solutions. Journal of the Taiwan

Institute of Chemical Engineers. 2016;63:312-7.
[34] Hanandeh AE, Abu-Zurayk RA, Hamadneh I, Al-Dujaili AH. Characterization of biochar prepared from slow pyrolysis of Jordanian olive oil processing solid waste and adsorption efficiency of Hg2+ ions in aqueous solutions. Water science and technology : a journal of the International Association on Water Pollution Research. 2016;74:1899-910.
[35] Inyang MI, Gao B, Yao Y, Xue Y, Zimmerman A, Mosa A, et al. A review of biochar as a low-cost adsorbent for aqueous heavy metal removal. Critical Reviews in Environmental Science and Technology. 2015;46:406-33.
[36] Xu X, Schierz A, Xu N, Cao X. Comparison of the characteristics and mechanisms of Hg(II) sorption by biochars and activated carbon. Journal of colloid and interface science. 2016;463:55-60.
[37] Kong H, He J, Gao Y, Wu H, Zhu X. Cosorption of phenanthrene and mercury(II) from aqueous solution by soybean stalk-based biochar. Journal of agricultural and food chemistry. 2011;59:12116-23.
[38] Tang J, Lv H, Gong Y, Huang Y. Preparation and characterization of a novel graphene/biochar composite for aqueous phenanthrene and mercury removal. Bioresource technology. 2015;196:355-63.
[39] Bi Y, Wang Y, Gao C. Straw resource quantity and its regional distribution in China. Journal of Agricultural Mechanization Research 32(3), 1-7. (in Chinese)
[40] Liu P, Ptacek CJ, Blowes DW, Landis RC. Mechanisms of mercury removal by biochars produced from different feedstocks determined using X-ray absorption spectroscopy. Journal of hazardous materials. 2016;308:233-42.
[41] Noh JS, Schwarz JA. Estimation of the point of zero charge of simple oxides by mass titration. Journal of colloid and interface science. 1989;130:157-64.
[42] Prahas D, Kartika Y, Indraswati N, Ismadji S. Activated carbon from jackfruit peel waste by H3PO4 chemical activation: Pore structure and surface chemistry characterization. Chemical Engineering Journal. 2008;140:32-42.
[43] Novak JM, Lima I, Xing BS, Gaskin JW, Steiner C, Das KC, et al. Characterization of designer biochar produced at different temperatures and their effects on a loamy sand. Annals of Environmental Science. 2009;3:195-206.
[44] Sing KSW. Reporting physisorption data for gas/solid systems with special reference to the determination of surface area and porosity (Recommendations 1984). Pure & Applied Chemistry. 2009;57:2201-18.
[45] González PG, Pliego-Cuervo YB. Adsorption of Cd(II), Hg(II) and Zn(II) from aqueous solution using mesoporous activated carbon produced from Bambusa vulgaris striata. Chemical Engineering Research and Design. 2014;92:2715-24.
[46] González-García P, Centeno TA, Urones-Garrote E, Ávila-Brande D, Otero-Díaz LC. Microstructure and surface properties of lignocellulosic-based activated carbons. Applied Surface Science. 2013;265:731-7.
[47] Wang P, Tang L, Wei X, Zeng G, Zhou Y, Deng Y, et al. Synthesis and application of iron and zinc doped biochar for removal of p -nitrophenol in wastewater and assessment of the influence of co-existed Pb(II). Applied Surface Science. 2017;392:391-401.
[48] Han Y, Boateng AA, Qi PX, Lima IM, Chang J. Heavy metal and phenol adsorptive properties of biochars from pyrolyzed switchgrass and woody biomass in correlation with surface properties. Journal of environmental management. 2013;118:196-204.
[49] Houben D, Sonnet P, Cornelis J-T. Biochar from Miscanthus: a potential silicon fertilizer. Plant and Soil. 2013;374:871-82.

[50] Yuan JH, Xu RK, Zhang H. The forms of alkalis in the biochar produced from crop residues at different temperatures. Bioresource technology. 2011;102:3488-97.
[51] Cui L, Wang Y, Gao L, Hu L, Wei Q, Du B. Removal of Hg(II) from aqueous solution by resin loaded magnetic beta-cyclodextrin bead and graphene oxide sheet: Synthesis, adsorption mechanism and separation properties. Journal of colloid and interface science. 2015;456:42-9.
[52] Kumar KV, Ramamurthi V, Sivanesan S. Modeling the mechanism involved during the sorption of methylene blue onto fly ash. Journal of colloid and interface science. 2005;284:14-21.
[53] Jin G, Eom Y, Lee TG. Removal of Hg(II) from aquatic environments using activated carbon impregnated with humic acid. Journal of Industrial and Engineering Chemistry. 2016;42:46-52.
[54] Bedin KC, Martins AC, Cazetta AL, Pezoti O, Almeida VC. KOH-activated carbon prepared from sucrose spherical carbon: Adsorption equilibrium, kinetic and thermodynamic studies for Methylene Blue removal. Chemical Engineering Journal. 2016;286:476-84.
[55] Deng L, Shi Z, Wang L, Zhou S. Fabrication of a novel NiFe2O4/Zn-Al layered double hydroxide intercalated with EDTA composite and its adsorption behavior for Cr(VI) from aqueous solution. Journal of Physics and Chemistry of Solids. 2017;104:79-90.
[56] Raghubanshi H, Ngobeni SM, Osikoya AO, Shooto ND, Dikio CW, Naidoo EB, et al. Synthesis of graphene oxide and its application for the adsorption of Pb+2 from aqueous solution. Journal of Industrial and Engineering Chemistry. 2017;47:169-78.
[57] Rao MM, Reddy DH, Venkateswarlu P, Seshaiah K. Removal of mercury from aqueous solutions using activated carbon prepared from agricultural by-product/waste. Journal of environmental management. 2009;90:634-43.
[58] Kołodyńska D, Krukowska J, Thomas P. Comparison of sorption and desorption studies of heavy metal ions from biochar and commercial active carbon. Chemical Engineering Journal. 2017;307:353-63.
[59] Wang T, Sun H. Biosorption of heavy metals from aqueous solution by UV-mutant Bacillus subtilis. Environmental science and pollution research international. 2013;20:7450-63.
[60] Perez-Marin AB, Ballester A, Gonzalez F, Blazquez ML, Munoz JA, Saez J, et al. Study of cadmium, zinc and lead biosorption by orange wastes using the subsequent addition method. Bioresource technology. 2008;99:8101-6.
[61] Srinivasan P, Sarmah AK, Smernik R, Das O, Farid M, Gao W. A feasibility study of agricultural and sewage biomass as biochar, bioenergy and biocomposite feedstock: Production, characterization and potential applications. Science of The Total Environment. 2015;512-513:495-505.
[62] Kılıç M, Keskin ME, Mazlum S, Mazlum N. Hg(II) and Pb(II) adsorption on activated sludge biomass: Effective biosorption mechanism. International Journal of Mineral Processing. 2008;87:1-8.